Research Paper Computational Methods for Differential Equations http://cmde.tabrizu.ac.ir Vol. *, No. *, *, pp. 1-19 DOI:10.22034/cmde.2025.66259.3085



Approximate analytical study on Maxwell and Williamson nonofluid flow

Vembu Ananthaswamy*, Manoharan Kalaivani, and Sathyamoorthy Sivasankari

Research Centre and PG Department of Mathematics, The Madura College (Affiliated to Madurai Kamaraj University), Madurai, Tamil Nadu, India.

Abstract

The motion of Maxwell and Williamson nanofluids across a decreasing surface with slip conditions is mathematically analyzed. The Modified Homotopy analysis methodology (MHAM) is deployed to tackle the governing transformed ordinary differential equations. Significant agreement is identified when comparing the obtained dimensionless approximate analytical solutions for temperature, concentration and velocity with the numerical result. A graphic illustration is delivered for the implications of numerous physical factors, including fluid factors, radiation, and slip factors. Both Maxwell and Williamson fluids' physical variables of importance, such as the skin friction factor, Sherwood and Nusselt number, are computed and presented in tabular form.

Keywords. Williamson fluid, Stagnation point flow, Shrinking sheet, Maxwell fluid, Modified Homotopy Analysis Method (MHAM). 2010 Mathematics Subject Classification. 34B60, 34E05, 34E10, 34E20.

1. Introduction

In recent decades, a lot of researchers have emphasized the emerging topic of non-Newtonian fluids owing to their numerous applications across numerous sectors. Fluids with different viscosities that are non-Newtonian are used in many medical and industrial applications. Non-Newtonian fluids are employed in a variety of industries due to their distinctive characteristics and performance, including the manufacturing and industrial processes, food and beverage industry, medicines and cosmetics, biomedical applications, and so on. Non-Newtonian fluids such as the Maxwell and Williamson fluid models are widely employed.

Maxwell fluids (MF) are generalized fluids that exhibit both viscous and elastic properties. Maxwell fluids (MF) are important because they allow us to understand and predict the motion of materials. Their ability to optimize system performance and boost system efficiency makes them essential. The Maxwell fluid flow model was first developed by Maxwell [21]. Within the thin film of an unsteady Maxwell fluid, Faraz and Khan [5] investigated the changing features of a flow and utilize Homotopy analysis method (HAM) to examine the impact of extending and contracting sheets. Azmi et al. [2] employed the Keller box strategy to explore the implications of a Maxwell hybrid nanofluid on blended convective radiative motion via an elongating/contracting inclined plate. The dynamics of constant-state MF motion were addressed by Ramar et al. [24], adopting the Runge-Kutta (RK) (BVP4C) approach, with specific view to the consequence of mass flux zero at the border and melting heat.

Under shear, Williamson fluid (WF) can thicken and thin because it is a pseudo-plastic fluid. Understanding the flow of the WF is essential to understanding biological processes like blood flow as well as the transport of mass and heat. Williamson [32] explained the flow of pseudoplastic liquids and supported his arguments with concrete data. For two exceptional situations, Nadeem and Hussain [23] exploited Optimal Homotopy analysis method (OHAM) to assess the consequences of heat transmission on the flow through the border layer of WF through a surface that is exponentially extending. The mass as well an heat transmission in Magnetohydrodynamic (MHD) Williamson nanofluid (WNF) motion responsive to mass suction and warmth production/ingestion was examined by Li et al. [14]

Received: 06 March 2025; Accepted: 02 November 2025.

^{*} Corresponding author. Email: ananthu9777@gmail.com.

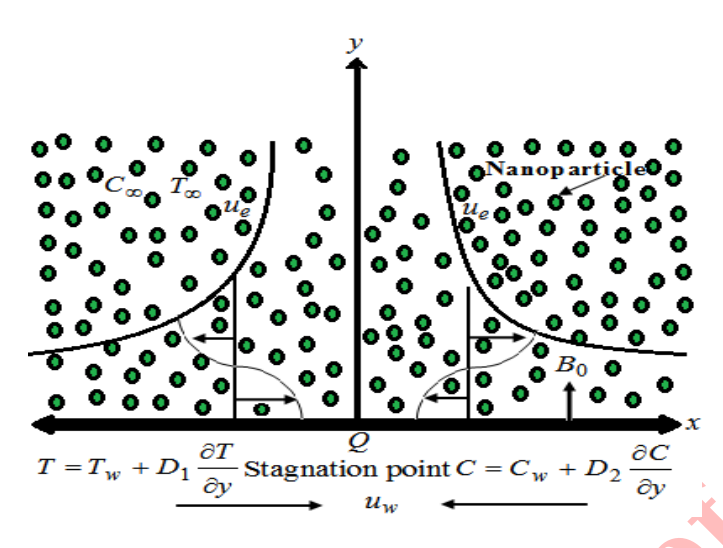


FIGURE 1. Physical structure of the flow.

employing byp4c in two different circumstances. Applying the modified wavelets method, Iqbal et al. [10] numerically investigated the moving MHD WNF movement exhibiting with changing thermal conductivity and diffusivity.

For the MHD border layer, Geetha et al. [6] executed the byp4c approach for assessing the WF motion in the context of a chemical response via a permeable enlarging/diminishing sheet. Implication of MHD motion through the border layer along an enlarging sheet has been studied by Nadeem et al. [22] via the RK4 approach. Ramesh and Gireesha's numerical results [25] provide insight into the Maxwell fluid's response properties when nanoparticles and a heat source/sink are present, utilizing RK4 with a shooting strategy. In order to address the equations pertaining to the motion of an upper convected MF having internal heat production/ingestion, Khan et al. [12] employed HAM. Swain et al. [30] adopted RK4 exhibiting shooting approach to examine how heat source/sink and thermal radiation affect 3D NF movement incorporated into a porous media involving aggregation of nanoparticles. Concurrent consequences of mass and transfer of heat in the motion of WF via an unstable elongating surface were evaluated by Hayat et al. [9] via HAM. A numerical analysis of the 2D MHD nano-Williamson fluid flow was conducted by Saleem and Hussain [27]. Kho et al. [13] assessed the border layer motion of WNF via an enlarging sheet in the occurrence of radiation implications via shooting technique.

The major goal of present work is to provide the semi-analytical responses for the temperature, concentration and velocity, equations regarding the stagnation point motion of the MNF and WNF via a diminishing surface exhibiting magnetic force and radiation via the Modified Homotopy analysis methodology. The outcomes are contrasted against a numerical result to show the proposed technique's accuracy. The implications of numerous factors engaged in the model are visually depicted. The physical factors are calculated and tabulated numerically.

2. Mathematical formulation of the problem

Consider the constant stagnation state motion of WNF and MNF's having the magnetic field and chemical response along a diminishing sheet [26]. In addition, the energy calculation takes the heat source into account. Figure 1 shows the motion, which is considered at y > 0. A diminishing surface moves with velocity $u_w = a x$, while the velocity of free stream is denoted by $u_e = a x$. A uniform temperature (T_w) and also concentration (C_w) are maintained over the plate's surface. The steady magnetic force of intensity B_0 was also adopted next to the flow's normal direction. T_{∞} specifies for the ambient temperature, and C_{∞} for the concentration.



The following are the equations that control continuation, momentum, strength, and also concentration [5, 8]:

$$\frac{\partial u}{\partial x} + \frac{\partial v}{\partial y} = 0, (2.1)$$

$$u\frac{\partial u}{\partial x} + v\frac{\partial u}{\partial y} = u_e \frac{\partial u_e}{\partial x} + \nu \frac{\partial^2 u}{\partial y^2} + \sqrt{2\nu} \Gamma \frac{\partial u}{\partial y} \frac{\partial^2 u}{\partial y^2} - \frac{\sigma B_0^2}{\rho} \left(u - u_e + v \frac{\partial u}{\partial y} K \right), \tag{2.2}$$

$$u\frac{\partial T}{\partial x} + v\frac{\partial T}{\partial y} = \alpha^* \left(1 + \frac{16\,\sigma^* T_\infty^3}{3k^*\,k} \right) \left(\frac{\partial^2 T}{\partial x^2} + \frac{\partial^2 T}{\partial y^2} \right) + \frac{Q_0}{\left(\rho c_p\right)_f} \left(T - T_\infty \right),$$

$$+\tau \left[D_B \left(\frac{\partial C}{\partial x} \frac{\partial T}{\partial x} + \frac{\partial C}{\partial y} \frac{\partial T}{\partial y} \right) + \frac{D_T}{T_\infty} \left(\left(\frac{\partial T}{\partial x} \right)^2 + \left(\frac{\partial T}{\partial y} \right)^2 \right)^2 \right], \tag{2.3}$$

$$u\frac{\partial C}{\partial x} + v\frac{\partial C}{\partial y} = D_B \left(\frac{\partial^2 C}{\partial x^2} + \frac{\partial^2 C}{\partial y^2}\right) + \frac{D_T}{T_{\infty}} + \zeta \left(C - C_{\infty}\right). \tag{2.4}$$

The respective boundary requirements exist outlined below [3, 4, 31]:

$$\begin{cases} v = v_w(x); & u = \lambda u_w(x), \quad T = T_w(x) + D_1 \frac{\partial T}{\partial y}, \quad C = C_w + D_2 \frac{\partial C}{\partial y}, \quad at \quad y = 0, \\ u \to u_e, \quad T \to T_\infty, \quad C \to C_\infty, \quad as \quad y \to \infty. \end{cases}$$
(2.5)

The velocity components in the y and x directions are represented by v and u, respectively. The shrinking sheet parameter is λ , D_1 , and D_2 are constants for the appropriate slip conditions. In order to prevent the fluid's inherent propensity to detach concerning the surface as it rapidly compresses, suction must exist for circulation over a diminishing surface. As a result, the boundary condition accounts for suction. Furthermore, temperature slip is a scientific phenomena that occurs when the temperature of a fluid flowing across a sheet is not thermally balanced with the sheet's temperature. Therefore, temperature as well concentration slip limits must used on the surface boundary.

The regulating Equations (2.1)–(2.5) are modified into dimensionless manner utilizing the similarity transformations stated below [7, 22]:

$$\begin{cases} u = a x F'(X), & v = -\sqrt{a v x} F'(X), & X = y \sqrt{\frac{a}{v}}, \\ T - T_{\infty} = (T_w - T_{\infty}) G(X), & and & C - C_{\infty} = (C_w - C_{\infty}) P(X). \end{cases}$$
(2.6)

When Eq. (2.6) is applied to the governing Eqs. (2.2)–(2.4) above, the transformed system is

$$F''' + FF'' - F'^2 + \beta \left(2FF'F'' - F^2F'''\right) + \gamma F''F''' + M\left(1 - F' + \beta FF''\right) + 1 = 0,$$
(2.7)

$$\left(1 + \frac{4}{3}R\right)G'' + Pr\left(FG' + NbG'P' + NtG'^2 + HG\right) = 0,$$
(2.8)

$$P'' + \left(\frac{Nt}{Nb}\right)G'' + ScFP' - ScQP = 0.$$

$$(2.9)$$

The boundary requirements are

$$\begin{cases}
F(0) = \epsilon, & F'(0) = \lambda, & \text{and } F'(\infty) \to 1, \\
G(0) = 1 + S_1 G'(0), & \text{and } G(\infty) \to 0, \\
P(0) = 1 + S_2 P'(0), & \text{and } P(\infty) \to 0,
\end{cases}$$
(2.10)

where $\beta=a\,K_1$ specifies Deborah number (MF factor), $\gamma=a\,x\,\Gamma\sqrt{\frac{2a}{\nu}}$ intensifies Williamson fluid parameter, $M=\frac{\sigma B_0^*}{a\rho}$ represents magnetic factor, $R=\frac{4\sigma^*T^3}{3k^*k}$ identifies radiation factor, $Pr=\frac{\nu}{a^*}$ denoted the Prandtl number, $Nb=\frac{\tau D_B(C_w-C_\infty)}{\nu}$ specifies the Brownian motion factor, $Nt=\frac{\tau D_T(T_w-T_\infty)}{\nu T_\infty}$ denotes the thermophoresis factor, $Q=\frac{\zeta}{a}$ identifies the chemical reaction factor, $Sc=\frac{\nu}{D_B}$ denotes the Schmidt number, $H=\frac{Q_0}{a\,\rho\,C_p}$ identifies the heat



source factor, $\epsilon = \frac{-v_w}{\sqrt{a\nu}}$ is mass (suction/injection) factor, $S_1 = D_1 \sqrt{\frac{a}{\nu}}$ and $S_2 = D_2 \sqrt{\frac{a}{\nu}}$ represents the thermal and concentration slip factors respectively.

2.1. **Physical quantities of interest:** The following relations can be utilized to figure out the friction factor coefficient, the rate of mass transmission, and heat transport for physical objects close to the wall.

$$Sh_x = \frac{x \, q_m}{D_B \left(C_w - C_\infty \right)}, \ Nu_x = \frac{x \, q_w}{k \left(T_w - T_\infty \right)}, \ and \ C_{f_x} = \frac{\tau_w}{\rho \, u_w^2}.$$
 (2.11)

where $q_m = -D_B \frac{\partial C}{\partial y}$ denotes the mass flux, $q_w = -\left(k + \frac{16\sigma^* T_{3k}^*}{3k^*}\right) \frac{\partial T}{\partial y}\Big|_{y=0}$ identifies the heat flux and $\tau_w = -\mu \left((1+\beta)\left(1 + \frac{\Gamma}{2}\frac{\partial u}{\partial y}\right) \frac{\partial u}{\partial y}\right)$ specifies the shear stress for the surface.

The dimensionless forms of the Sherwood, Nusselt number and skin friction factor remain as follows:

$$\begin{cases} Sh_x \left(Re_x \right)^{-\frac{1}{2}} = -P'(0), \ Nu_x \left(Re_x \right)^{-\frac{1}{2}} = -\left(1 + \frac{4}{3}R \right) G'(0), \\ and \ C_{f_x} \left(Re_x \right)^{\frac{1}{2}} = \left(1 + \beta \right) \left(1 + \frac{\gamma}{2} F''(0) \right) F''(0). \end{cases}$$
(2.12)

In this case, $\beta = 0.1$ and $\gamma = 0$ serve as the Maxwell fluid model, whereas $\beta = 0$ and $\gamma = 0.1$ reflect the Williamson fluid model.

3. Semi-analytical solution utilizing the Modified Homotopy Analysis Methodology (MHAM)

To explore non-linear issues that occur in the physical studies, particularly flow issues, a variety of analytical methods have been proposed. A Homotopy analysis approach was recommended by Liao [15–19] for handling very difficult non-linear problems that occur in the applied sciences. It serves as a non-perturbative mathematical methodology for finding series results for non-linear equations. According to Liao's work [15–19], prior HAM implementations have mostly focused on non-linear DEs that can be defined by polynomials of this kind. It reveals an analytical solution based on a power series with an unlimited number of terms. Nevertheless, this finding needs to be further evaluated, and the infinite power series needs to be used to compute values.

Modified Homotopy analysis methodology (MHAM) identifies a semi-analytical strategy that allows us to find the semi-analytical expressions for the non-linear differential equations regarding the flow problems. The dimensionless velocity, temperature, and concentration can all be mathematically expressed in a dimensionless way using MHAM [1, 20, 28, 29]. Following that, the whole derivation can be stated.

3.1. Semi-analytical expression for velocity, temperature and concentration utilizing Modified Homotopy Analysis Methodology (MHAM). The following describes the Homotopy for Eqs. (2.7) and (2.9).

$$(1-r)(F'''-F') = hr(F''' + FF'' - F'^2 + \beta(2FF'F'' - F^2F''') + \gamma F''F''' + M(1-F' + \beta FF'') + 1),$$
(3.1)

$$(1-r)(G''-G) = hr\left(\left(1 + \frac{4}{3}R\right)G'' + Pr\left(FG' + NbG'P' + NtG'^2 + HG\right)\right),\tag{3.2}$$

$$(1-r)\left(P''-P\right) = h r \left(P'' + \left(\frac{Nt}{Nb}\right)G'' + ScFP' - ScQP\right). \tag{3.3}$$

For Eqs. (3.1) and (3.3), the initial approximation is defined by

$$\begin{cases}
F_0(0) = \epsilon, & F'_0(0) = \lambda \text{ and } F'_0(\infty) \to 1, \\
G_0(0) = 1 + S_1 G'_0(0) \text{ and } G_0(\infty) \to 0, \\
P_0(0) = 1 + S_2 P'_0(0), \text{ and } P_0(\infty) \to 0,
\end{cases}$$
(3.4)



$$F_{i}(0) = 0, \quad F'_{i}(0) = 0 \quad and \quad F'_{i}(\infty) \to 0,$$

$$G_{i}(0) - S_{1}G'_{i}(0) = 0 \quad and \quad G_{i}(\infty) \to 0,$$

$$P_{i}(0) - S_{2}P'_{i}(0) = 0, \quad and \quad P_{i}(\infty) \to 0,$$

$$(3.5)$$

The semi-analytical resolutions for Eqs. (3.1) and (3.3) are represented below:

$$F = F_0 + rF_1 + r^2F_2 + \dots, (3.6)$$

$$G = G_0 + rG_1 + r^2G_2 + \dots, (3.7)$$

$$P = P_0 + rP_1 + r^2P_2 + \dots (3.8)$$

Putting the Eqs. (3.6)–(3.8) into Eqs. (3.1)–(3.3) and contrasting the coefficients of similar powers of r, we have: Initial iteration:

$$r^0: F_0''' - F_0' = 0, (3.9)$$

$$r^0: G_0'' - G_0 = 0, (3.10)$$

$$r^0: P_0'' - P_0 = 0. (3.11)$$

First iteration:

$$r^{1}: F_{1}^{"''} - F_{1}^{'} - F_{0}^{"'} + F_{0}^{'}$$

$$= h \left(F_{0}^{"''} + F_{0}F_{0}^{"} - F_{0}^{'2} + \beta \left(2F_{0}F_{0}^{'}F_{0}^{"'} - F_{0}^{2}F_{0}^{"'} \right) + \gamma F_{0}^{"}F_{0}^{"'} + M \left(1 - F_{0}^{'} + \beta F_{0}F_{0}^{"} \right) + 1 \right), \tag{3.12}$$

$$r^{1}: G_{1}^{"} - G_{1} - G_{0}^{"} + G_{0} = h\left(\left(1 + \frac{4}{3}R\right)G_{0}^{"} + Pr\left(F_{0}G_{0}^{'} + NbG_{0}^{'}P_{0}^{'} + NtG_{0}^{'2} + HG_{0}\right)\right),\tag{3.13}$$

$$r^{1}: P_{1}^{"} - P_{1} - P_{0}^{"} + P_{0} = h \, r \left(P_{0}^{"} + \left(\frac{Nt}{Nb} \right) G_{0}^{"} + Sc \, F_{0} P_{0}^{\prime} - Sc \, Q \, P_{0} \right). \tag{3.14}$$

At this point, the initial guessing results for Eqs. (3.9)-(3.11), which meet the requirements for the boundary in Eq. (3.4), are provided by exploring MHAM:

$$F_0(X) = \epsilon + X + \frac{(1-\lambda)}{N} \left(e^{-NX} - 1 \right),$$
 (3.15)

$$G_0(X) = \frac{1}{1 + S_1 A} e^{-AX},$$

$$P_0(X) = \frac{1}{1 + S_2 B} e^{-BX}.$$
(3.16)

$$P_0(X) = \frac{1}{1 + S_2 B} e^{-BX}. (3.17)$$

where

$$N = \sqrt{1 + \beta + \gamma + M}, \quad A = \sqrt{1 + \frac{Pr(H + Nt + Nb)}{\left(1 + \frac{4}{3}R\right)}}, \quad B = \sqrt{1 + Sc + \frac{Nt}{Nb} + Sc Q}.$$
 (3.18)

On solving Eqs. (3.12)-(3.14) with the use of Eqs. (3.15)-(3.17) and utilizing Eq. (3.5), we get the following results:

$$F_1(X) = C_1 + C_2 e^{-X} + A_1 e^{-NX} + A_2 e^{-2NX} + A_3 e^{-3NX} + A_4 X e^{-NX},$$
(3.19)

$$G_1(X) = C_3 e^{-X} + A_5 e^{-AX} + A_6 e^{-2AX} + A_7 e^{-(A+B)X} + A_8 e^{-(N+A)X} + A_9 X e^{-AX},$$
(3.20)

$$P_1(X) = C_4 e^{-X} + A_{10} e^{-BX} + A_{11} e^{-AX} + A_{12} e^{-(N+B)X} + A_{13} X e^{-BX},$$
(3.21)



where

$$\begin{cases}
C_{2} = -NA_{1} - 2NA_{2} - 3N A_{3} + A_{4}, & C_{1} = -C_{2} - A_{1} - A_{2} - A_{3}, \\
A_{1} = \frac{h(1-\lambda)}{-N^{3} + N} \left(-N^{2} + \left(\epsilon - \frac{1-\lambda}{N}\right) N \left(1 + 2\beta + M\beta\right) \right) \\
+ \frac{h(1-\lambda)}{-N^{3} + N} \left(\beta N^{2} \left(\epsilon^{2} - \left(\frac{1-\lambda}{N}\right)^{2} \right) - 2\beta N\epsilon(1-\lambda) + M + 1 \right) \\
+ \frac{h N(1-\lambda)(1-3N^{2})}{(N^{3} - N)^{2}} \left(1 + 2\beta + 2\beta N\epsilon - 2\beta(1-\lambda) + M\beta \right), \\
A_{2} = \frac{h(1-\lambda)^{2}}{-8N^{3} + 2N} \left(2\beta - 2\beta N \left(\epsilon - \frac{1-\lambda}{N} \right) - 2\beta(1-\lambda) + 2\beta N - \gamma N^{3} + M\beta \right), \\
A_{3} = \frac{-h\beta(1-\lambda)^{3}}{-27N^{3} + 3N}, & A_{4} = \frac{h N(1-\lambda)}{N^{3} + N} \left(1 + 2\beta + 2\beta N\epsilon - 2\beta(1-\lambda) + M\beta \right),
\end{cases} \tag{3.22}$$

$$\begin{cases}
A_{5} = \frac{h}{(A^{2} - 1)(1 + S_{1}A)} \left(\left(1 + \frac{4}{3}R \right) A^{2} - Pr A \left(\epsilon - \frac{1 - \lambda}{N} \right) + H Pr \right) + \frac{2h Pr A}{(A^{2} - 1)^{2}}, \\
A_{6} = \frac{h Pr Nt A^{2}}{(4A^{2} - 1)(1 + S_{1}A)}, \quad A_{7} = \frac{h Pr A B Nb}{((A + B)^{2} - 1)(1 + S_{1}A)(1 + S_{2}B))}, \\
A_{8} = \frac{-h Pr(1 - \lambda)A}{N(1 + S_{1}A)((N + A)^{2} - 1)}, \quad A_{9} = \frac{-h Pr A}{A^{2} - 1}, \\
C_{3} = \frac{-1}{1 + S_{1}A} \left(A_{5} + A_{6} + A_{7} + A_{8} - S_{1}(-A_{5}A - 2A_{6}A - (A + B)A_{7} - (N + A)A_{8} + A_{9}) \right),
\end{cases}$$

$$(3.23)$$

$$\begin{cases}
A_{10} = \frac{h}{(B^2 - 1)(1 + S_2 B)} \left(B^2 - B\epsilon Sc + \frac{ScB(1 - \lambda)}{N} - ScQ \right) + \frac{2hB^2Sc}{(B^2 - 1)^2(1 + S_2 B)}, \\
A_{11} = \frac{hA^2Nt}{Nb(A^2 - 1)(1 + S_1 A)}, \quad A_{12} = \frac{-hScB(1 - \lambda)}{N((N + B)^2 - 1)(1 + S_2 B)}, \quad A_{13} = \frac{-hScB}{(B^2 - 1)(1 + S_2 B)}, \\
C_4 = \frac{1}{1 + S_2} \left(-A_{10} - A_{11} + A_{12} + S_2 \left(-BA_{10} - A_{11}A - (N + B)A_{12} + A_{13} \right) \right).
\end{cases} (3.24)$$

As per the HAM methodology, we possess

$$F = \lim_{X \to 0} F(X) = F_0 + F_1, \tag{3.25}$$

$$G = \lim_{X \to X} G(X) = G_0 + G_1, \tag{3.26}$$

$$P = \lim_{X \to 0} P(X) = P_0 + P_1. \tag{3.27}$$

Hence, the responses of the velocity, temperature and also concentration equations are retrieved by putting Eqs. (3.15) to (3.17) and (3.19)-(3.21) into Eqs. (3.25)-(3.27), as follows:

$$F(X) = \epsilon + X + \frac{(1-\lambda)}{N} \left(e^{-NX} - 1 \right) + C_1 + C_2 e^{-X} + A_1 e^{-NX} + A_2 e^{-2NX} + A_3 e^{-3NX} + A_4 X e^{-NX},$$
 (3.28)

$$G(X) = \frac{1}{1 + S_1 A} e^{-AX} + C_3 e^{-X} + A_5 e^{-AX} + A_6 e^{-2AX} + A_7 e^{-(A+B)X} + A_8 e^{-(N+A)X} + A_9 X e^{-AX}, \tag{3.29}$$

$$G(X) = \frac{1}{1 + S_1 A} e^{-AX} + C_3 e^{-X} + A_5 e^{-AX} + A_6 e^{-2AX} + A_7 e^{-(A+B)X} + A_8 e^{-(N+A)X} + A_9 X e^{-AX},$$
(3.29)

$$P(X) = \frac{1}{1 + S_2 B} e^{-BX} + C_7 e^{-X} + A_{10} e^{-BX} + A_{11} e^{-AX} + A_{12} e^{-(N+B)X} + A_{13} X e^{-BX},$$
(3.30)

where the terms N, A, B, A_8 , A_1 , C_1 , A_2 , A_{11} , A_3 , A_4 , C_2 , A_5 , A_6 , A_{10} , A_7 , A_9 , A_{12} , C_3 , A_{13} and C_4 are defined in Eqs. (3.18), (3.22), (3.23), and (3.24).



3.2. Semi-analytical expressions for physical quantities of interest. The semi-analytical expressions for the skin friction factor, Nusselt and also Sherwood number are given as follows:

$$C_{f_x} (Re_x)^{\frac{1}{2}} = (1+\beta) \left(1 + \frac{\gamma}{2} F''(0)\right) F''(0)$$

$$= (1+\beta) \left(1 + \frac{\gamma}{2} \left(N(1-\lambda) + C_2 + N^2(A_1 + 4A_2 + 9A_3) - 2NA_4\right)\right), \tag{3.31}$$

$$Nu_x (Re_x)^{-\frac{1}{2}} = -\left(1 + \frac{4}{3}R\right)G'(0)$$

$$= \left(1 + \frac{4}{3}R\right) \left(\frac{A}{1 + S_1A} + C_3 + A(A_5 + 2A_6) + (A + B)A_7 + (N + A)A_8 - A_9\right),\tag{3.32}$$

$$Sh_x (Re_x)^{-\frac{1}{2}} = -P'(0) = \frac{B}{1 + S_2 B} + C_7 + BA_{10} + A_{11}A + (N+B)A_{12} - A_{13}.$$
(3.33)

4. Results and discussion

With a graphic illustration, this section provides a detailed explanation of the various physical components that comprise the model. The semi-analytical results utilizing Eqs. (3.28)–(3.30) are contrasted against the numerical responses using the Galerkin weighted residual technique, as previously mentioned [26]. In comparison to the numerical methodology, our solutions are more reliable and converge more quickly. The results are explained in complete detail in the paragraphs that follow.

The graph assume the following constant values for each parameters: Pr=2, M=0.2, $\beta=\gamma=Rd=S_1=0.1$, Nb=Nt=0.4, Sc=3, $\lambda=-1$, $S_1=0.5$, $\epsilon=1.8$.

Figures 2 through 4 compare semi-analytical results with numerical solutions for temperature, concentration, and dimensionless velocity, respectively for some fixed values of the parameters. The figures presented here portray that the semi-analytical outcome and the numerical response (previous work) agree quite well for both Williamson and Maxwell fluids.

For velocity distribution: Figures 5 and 6 compare the semi-analytical results using Eq. (3.28) and the numerical response reported in [26] of the velocity profile F'(X) in non-dimensional form for varying amounts of ϵ and M. Since the Lorentz force improves the fluid's motion in the border layer state, Figure 5 demonstrates that velocity rises when the suction factor rises. Consequently, the momentum border layer's thickness gets drop. Furthermore, the MNF's velocity is still less than WNF. A rise in the magnetic component causes the velocity to increase in Figure 6. The MNF's velocity is obviously higher than WNF. As a fluid travels and confronts electrical and magnetic forces, the Lorentz force is produced, which exacerbates this.

For temperature distribution: Figures 7 to 11 indicate a comparison of semi-analytical outcomes by Eq. (3.29) and numerical results presented in [26] of the temperature G(X) in a non-dimensional state for diverse amounts of ϵ , S_1 , Pr, Nt and H. Figure 7 depicts that when the suction factor boosts, the temperature falls. Suction prevents the thermal border layer from becoming thick by acquiring the fluid adjacent to the surface at ambient temperature. In addition, the MNF profile is seen to be lower relative to WNF profile. As displayed in Figure 8, when the slip factor gets higher, temperature goes down. Also, the WNF has a higher thermal profile than the MNF. The potential for the thermal slip factor to drop is responsible for this. Figure 9 shows how the temperature declines as Prapproaches. WNF has a higher temperature than MNF. Based on a physical point of view, this anomaly implies a drop in fluid temperature that triggers a fall in thermal conductivity. The fluid has an intrinsic feature known as the dimensionless Prandtl number. Fluids that flow freely have a low Pr and strong heat conductivity. Pr calculates the respective thicknesses of the thermal and also momentum border layers. Because Pr indicates the association of thermal conductivity and momentum diffusivity, rising Pr reduces thermal conductivity. Figure 10 illustrates that increasing the amount of thermophoresis factor causes the temperature to rise. Moreover, the temperature properties of MNF are higher relative to those of WNF. Different fluid particles physically react moderate to variations in Ntdue to the presence of a temperature. Particles start to travel faster as Nt increases, which raises the system's kinetic energy and raises the border layer's thickness and internal temperature distribution. As can be observed in Figure 11, the temperature improves as the heat source component rises. Since the positive heat generation component (H)



λ	Kameswaran et al. [11]	Prior work [26]	Present study (3.32)
0	0.8113013	0.81130063	0.81121787
-0.25	0.6685728	0.66857187	0.66854899
-0.5	0.5014476	0.50144774	0.50144352
-0.75	0.2931625	0.29316239	0.29316105

Table 1. Comparison of Nu_x with previous works.

renders warmth in the fluid circulation, the temperature curves physically improve when it gets stronger. Furthermore, the profile of MNF is marginally worse than WNF.

For concentration distribution: Figures 12 to 15 indicate a comparison of analytical outcomes by Eq. (3.30) and numerical results presented in [26] of the concentration profile P(X) in a non-dimensional state for diverse amounts of ϵ , Pr, Nt, Nb, Sc, S_1 , Q and S_2 . The concentration properties of both fluids are shown in Figure 12 to drop as the suction factor improves. In contrast to WNF, MNF has a worse quality. This is why suction lowers the concentration thickness of the barrier layer's thickness by drawing the fluid situated to the surface. According to Figure 13, the concentration declines when the amount of Pr enhances. As can be identified in Figure 14, the concentration goes up as Nt is raised. Additionally, a little change in Nt affect the movement of fluid particles rapidly, which results in excess heat energy and a significant raise in concentration changes. By boosting the amount of Nb, Figure 15 illustrates how P(X) diminishes. A raise in Nb accelerates unexpected motion, dispersing the nanoparticles and causing a decline in concentration. In the meantime, WNF has a better concentration than MNF. Figure 16 displays the concentration falls by boosting the amount of Sc. Sc is a metric for the ratio of mass diffusivity to momentum. Therefore, in the concentration and hydrodynamic border layers, Sc quantifies the efficiency of mass transmission by diffusion and also momentum transport. When Sc > 1, the rate of momentum diffusion is greater than the species and when Sc < 1, the opposite is true. For Sc=1, the thickness of the species and momentum barrier layers remain equal, as will the rate of diffusivity. Reducing amounts of Sc are associated with improving a chemical molecule's diffusivity, where as bigger amounts of Sc are associated with the opposite effect. Consequently, the concentration barrier layer's thickness declines dramatically if Sc rises. In addition, the concentration profile of WNF is higher than MNF. According to Figure 17, the concentration drops when the amount of slip parameter goes up. Furthermore, contrasted to the WNF, the MNF's associated profile is marginally lower. Figure 18 interlines that by boosting the amount of heat source (reaction) factor, the concentration drops. WNF has a similar but higher concentration profile than MNF. The chemical response that occurs in the model results in chemical consumption, which causes the concentration profile to decline. Figure 19 demonstrates the concentration falls by enhancing the amount of the concentration slip factor. Additionally, MNF is better impacted by S_2 than WNF. Slip basically reduces the fluid velocity, which lowers net molecular movement, which is why this is to be expected. In turn, when molecular mobility declines, mass fraction fields also ruins.

For physical quantities of interest: We check the method's accuracy by contrasting the present outcomes with the previously reported information in Table 1, and we find that they are in good agreement with the earlier studies for varying amounts of shrinking sheet parameter on Nu_x . Table 2 provides the implications of the shrinkage, suction, and magnetic surface characteristics on the skin friction factor using Eq. (3.31) for the two nanofluids. In fact, the numerical amounts of C_{f_x} obviously goes up when the suction and also magnetic factors improve. C_{f_x} amounts rises numerically as λ drops. Clearly, when expressed numerically, the amount is a bit more for MNF than WNF. The Nusselt number amount utilizing Eq. (3.32) for various Pr, Rd and H amounts is outlined in Table 3. The amount of Nu_x falls as the heat source factor and Pr rise. At WNF, this is a little lower. The Nusselt number also gets stronger as the radiation factor raises. Table 4 indicates the amount of Sh_x utilizing Eq. (3.33) for numerous amounts of Sc, Nb and S_2 . As Nb and S_2 concentrations raise, Sh_x drops. Interestingly, Sh_x quantities also rise when the amount of Sc grows.



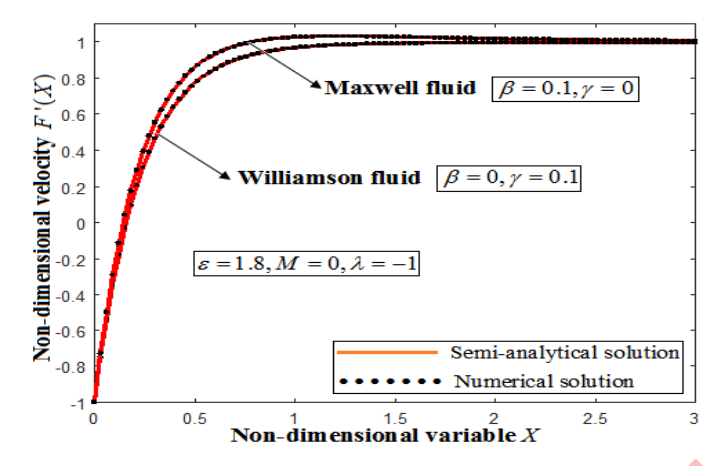


FIGURE 2. Dimensionless velocity F'(X) versus dimensionless variable X. Comparison between semi-analytical results using Eq. (3.28) for the velocity profile with a numerical solution.

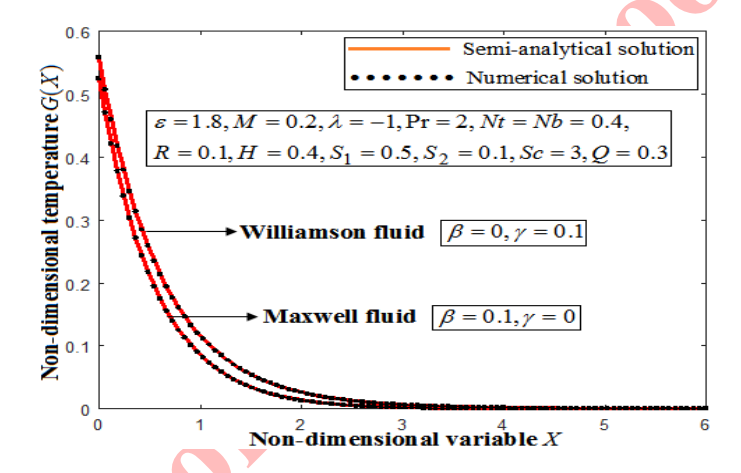


FIGURE 3. Dimensionless temperature G(X) versus dimensionless variable X. Comparison between semi-analytical results using Eq. (3.29) for the temperature profile with a numerical solution.

5. Conclusion

We mathematically assessed of the motion of MNF and WNF's via a diminishing surface having slip conditions. The regulating converted ordinary differential equations were tackled utilizing the MHAM. The attained semi-analytical responses were contrasted with numerical strategy results in remarkable agreement for temperature, velocity and concentration in dimensionless form. The influences of several physical factors, specifically radiation, slip factors, and fluid factor, were depicted graphically. The physical quantities, like the skin friction factor, Sherwood, and Nusselt number, for both MNF and WNF were calculated and shown in tabular form. The following discoveries evolved from the findings:

- Magnetic force and suction parameter enhance non-dimensional velocity.
- Suction, Prandtl number, and thermal slip parameters have negative implications on non-dimensional temperature, whereas thermophoresis and heat source characteristics have a positive effect.
- By increasing the thermophoresis parameter, dimensionless concentration rises; however, by increasing the suction, Prandtl, Schmidt, Brownian motion, chemical reaction rate, thermal slip, and concentration slip parameters, it falls.



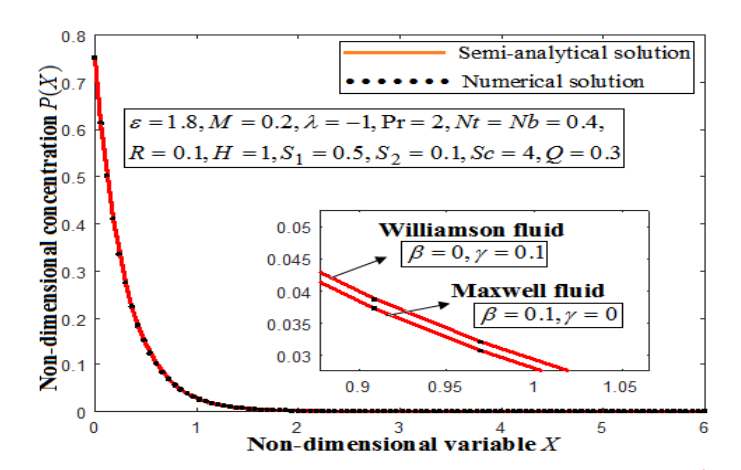


FIGURE 4. Dimensionless concentration P(X) versus dimensionless variable X. Comparison between semi-analytical results using Eq. (3.30) for the concentration profile with a numerical solution.

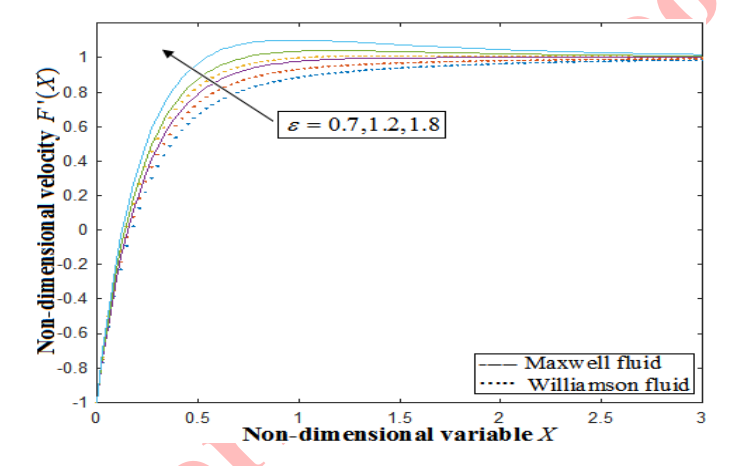


FIGURE 5. Dimensionless velocity F'(X) versus dimensionless variable. Effects of suction parameter on F'(X) using Eq. (3.28).

• Making use of MHAM for addressing the equation for the Williamson and Maxwell nanofluid is an immensely valuable approach. Both the semi-analytical along with numerical estimates agree to a considerable extent.

Conflict of interests

The authors declare that there is no conflict of interests.

ACKNOWLEDGEMENT

The authors are very grateful to the reviewers for carefully reading the paper and for their comments and suggestions which have improved the paper. Also, the authors are thankful to Sri. S. Natanagopal, Secretary, The Madura College Board, Dr. J. Suresh, The Principal, The Madura College and Dr. C. Thangapandi, Head of the Department, The Madura College, Madurai, Tamil Nadu, India for their constant support to our research work.



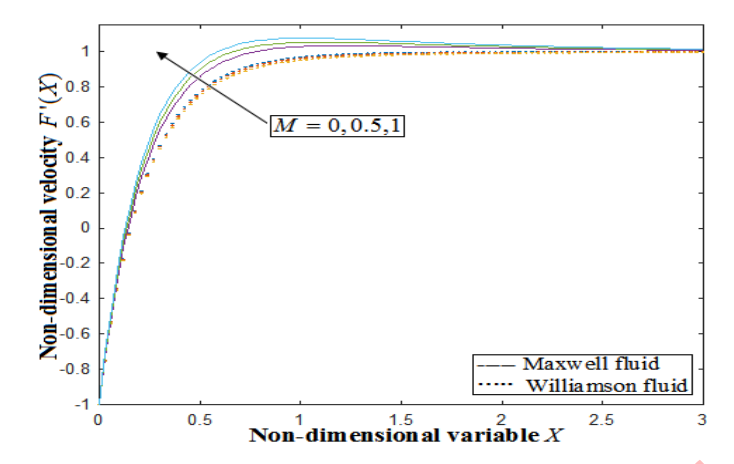


FIGURE 6. Dimensionless velocity F'(X) versus dimensionless variable. Influence of magnetic field parameter on F'(X) using Eq. (3.28).

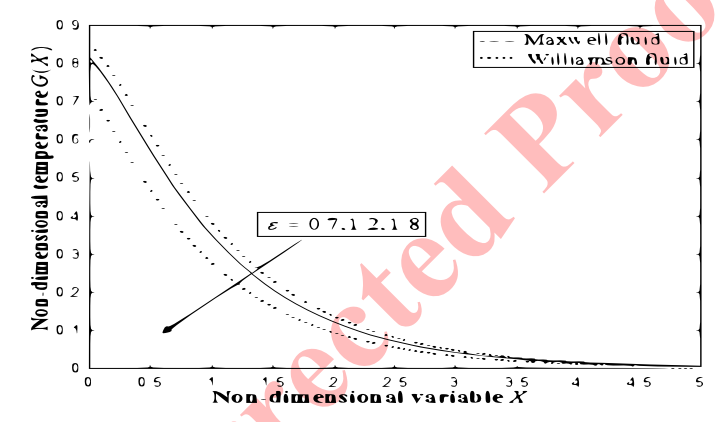


FIGURE 7. Dimensionless temperature G(X) versus dimensionless variable. Consequences of suction field parameter on G(X) using Eq. (3.29).

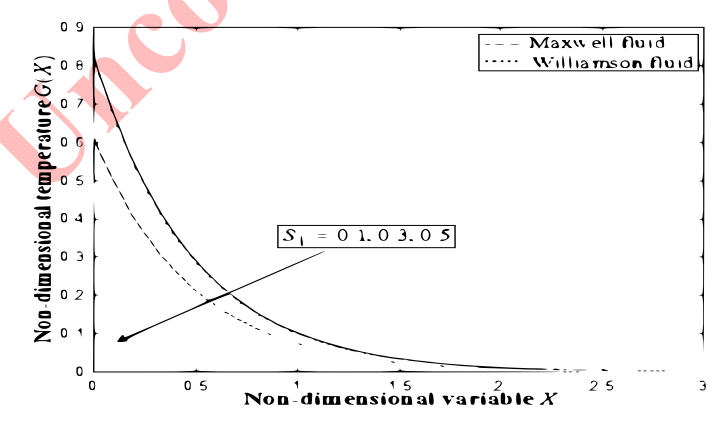


FIGURE 8. Dimensionless temperature G(X) versus dimensionless variable. Impacts of thermal slip parameter on G(X) using Eq. (3.29).



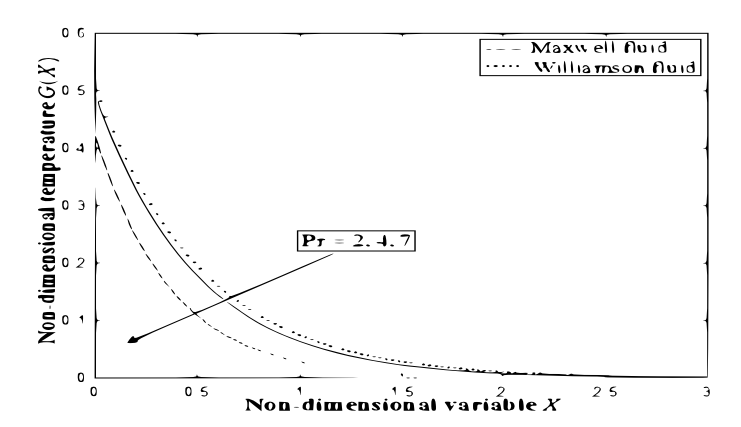


FIGURE 9. Dimensionless temperature G(X) versus dimensionless variable. Implications of Prandtl number on G(X) using Eq. (3.29).

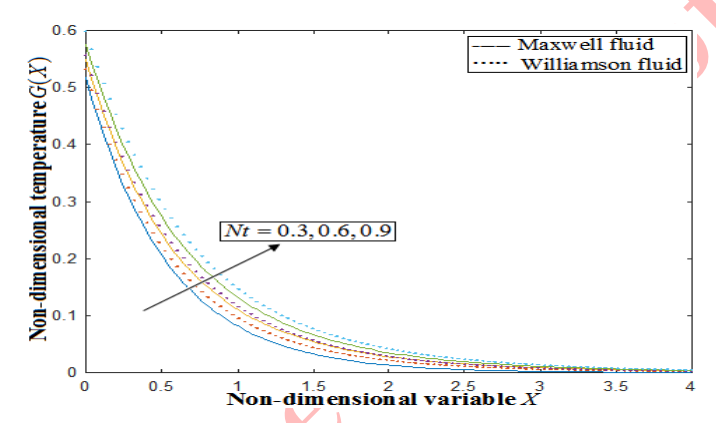


FIGURE 10. Dimensionless temperature G(X) versus dimensionless variable. Influence of thermophoresis parameter on G(X) using Eq. (3.29).

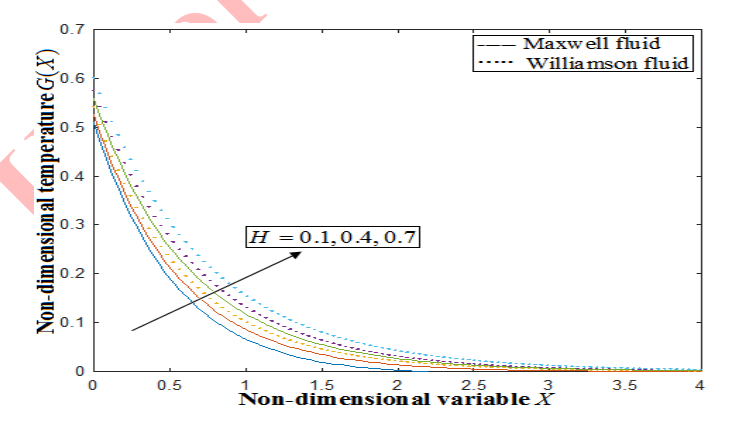


FIGURE 11. Dimensionless temperature G(X) versus dimensionless variable. Impacts of heat source parameter on G(X) using Eq. (3.29).



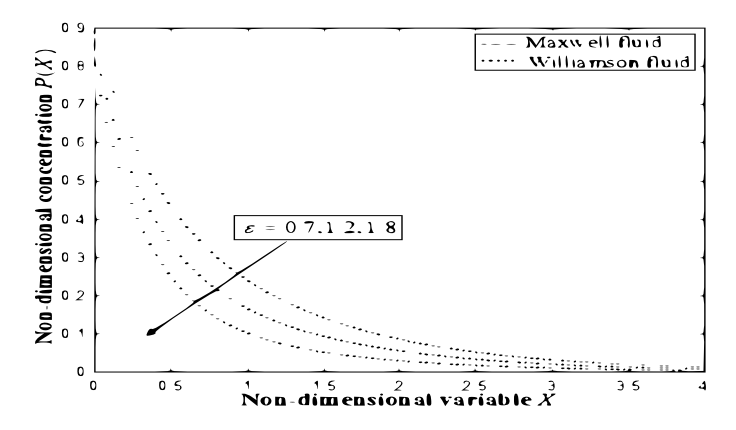


FIGURE 12. Dimensionless concentration P(X) versus dimensionless variable. Consequences of suction parameter on P(X) using Eq. (3.30).

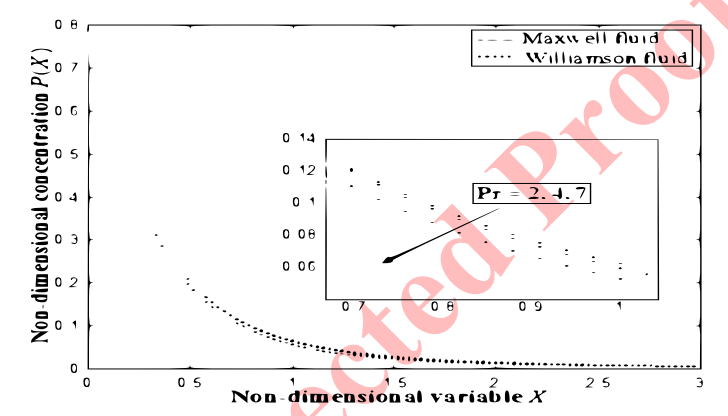


FIGURE 13. Dimensionless concentration P(X) versus dimensionless variable. Implications of Prandtl number on P(X) using Eq. (3.30).

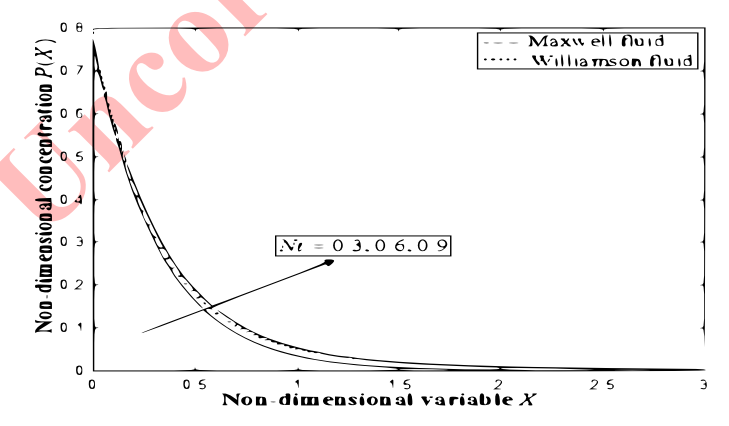


FIGURE 14. Dimensionless concentration P(X) versus dimensionless variable. Influence of thermophoresis parameter on P(X) using Eq. (3.30).



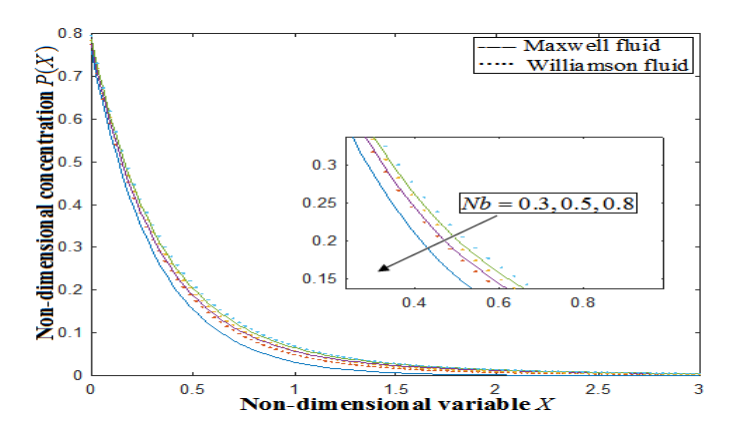


FIGURE 15. Dimensionless concentration P(X) versus dimensionless variable. Variations of Brownian motion parameter on P(X) using Eq. (3.30).

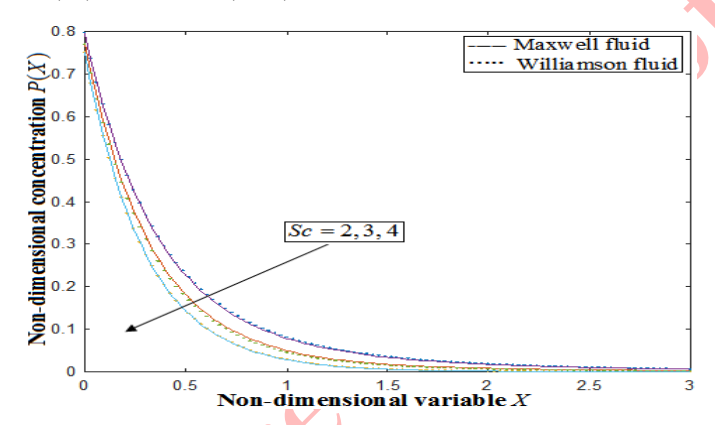


FIGURE 16. Dimensionless concentration P(X) versus dimensionless variable. Effects of Schmidt number on P(X) using Eq. (3.30).

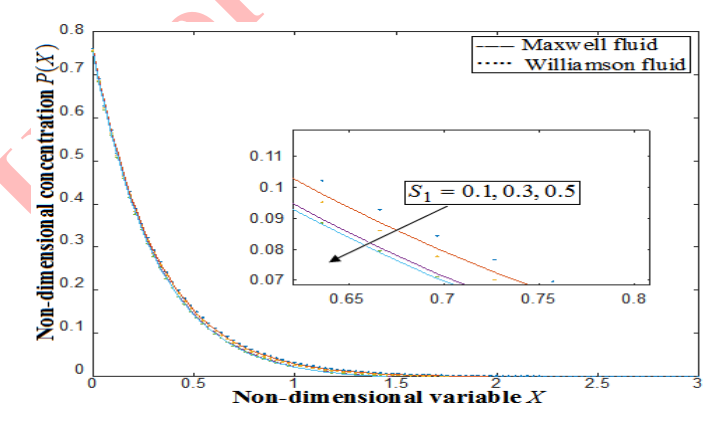


FIGURE 17. Dimensionless concentration P(X) versus dimensionless variable. Impacts of thermal slip parameter on P(X) using Eq. (3.30).



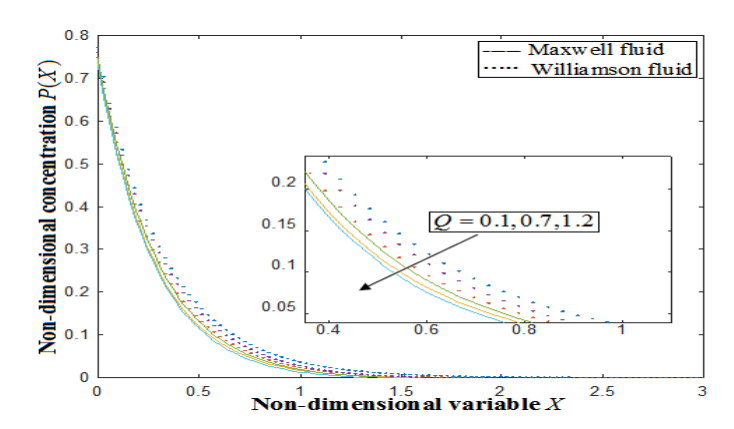


FIGURE 18. Dimensionless concentration P(X) versus dimensionless variable. Consequences of chemical reaction parameter on P(X) using Eq. (3.30).

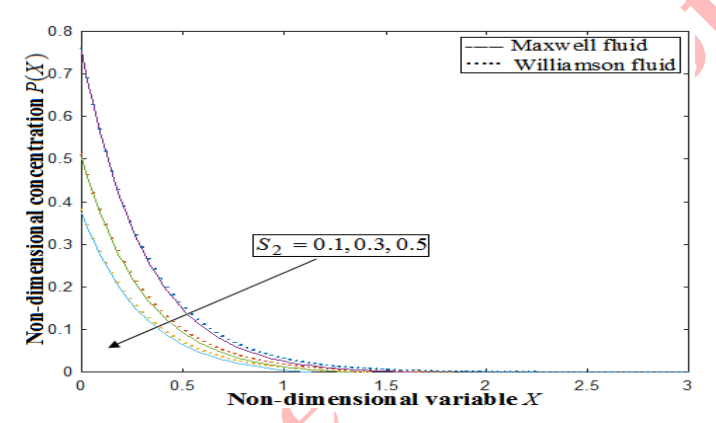


FIGURE 19. Dimensionless concentration P(X) versus dimensionless variable. Variations of concentration slip parameter on P(X) using Eq. (3.30).

Table 2. Comparison of Nu_x with previous work.

Parameter values	Maxwell fluid			Williamson fluid		
rarameter values	MHAM Solution	Numerical Solution [26]	Error %	MHAM Solution	Numerical Solution [26]	Error %
M = 0	-1.503989	-1.503933	0.003724	-1.346405	-1.346508	0.007649
M = 0.1	-1.642160	-1.642167	0.000426	-1.469647	-1.4697797	0.008981
M = 0.5	-2.096603	-2.097361	0.036141	-1.857699	-1.857731	0.001723
$\epsilon = 0.1$	-1.641919	-1.642167	0.015102	-1.468584	-1.469779	0.081305
$\epsilon = 0.6$	-2.443047	-2.443943	0.036662	-2.030372	-2.030885	0.025259
$\epsilon = 1.2$	-4.320407	-4.321372	0.022331	-2.700058	700098	0.001481
$\lambda = -0.25$	-1.575987	-1.576049	0.003934	-1.401425	-1.401532	0.007635
$\lambda = -0.50$	-1.691597	-1.691948	0.020745	-1.507949	-1.509598	0.109234
$\lambda = -0.75$	-1.721291	-1.721707	0.024162	-1.541974	-1.542017	0.002789
Absolute average error percentage			0.018136			0.027339



Table 3. Comparison of C_{f_x} with previous work.

Parameter values	Maxwell fluid			Williamson fluid		
r arameter values	MHAM Solution	Numerical Solution [26]	Error %	MHAM Solution	Numerical Solution [26]	Error %
Pr = 1	0.135148	0.135442	0.217067	0.111038	0.111052	0.012606
Pr = 2	0.0130611	0.013062	0.006890	-0.016976	-0.017928	5.305109
Pr = 3	-0.102825	-0.103237	0.399082	-0.153689	-0.153797	0.070222
Rd = 0.1	0.013021	0.013062	0.348348	0.013458	0.013597	1.022284
Rd = 0.2	0.0492897	0.049462	0.348348	0.013458	0.013597	1.022284
Rd = 0.3	0.0901689	0.090681	0.564727	0.048500	0.048531	0.063877
H = 0.1	0.158009	0.158030	0.013288	0.137218	0.137231	0.009473
H = 0.2	0.0130596	0.013062	0.018374	-0.017903	-0.017928	0.138331
H = 0.3	-0.197705	-0.197793	0.044491	-0.242275	-0.242292	0.007016
Absolute average error percentage			0.214017			0.793565

Table 4. Comparison of Sh_x with previous work.

Parameter values	Maxwell fluid		Williamson fluid			
rarameter values	MHAM Solution	Numerical Solution [26]	Error %	MHAM Solution	Numerical Solution [26]	Error %
Nb = 0.2	1.092488	1.092514	0.002379	1.064569	1.064578	0.000845
Nb = 0.4	0.944314	0.944337	0.002436	0.913156	0.913172	0.001752
Nb = 0.6	0.891223	0.891224	0.000112	0.860455	0.860611	0.018126
Sc = 1	0.722231	0.722545	0.043458	0.712649	0.712712	0.008839
Sc = 2	0.854334	0.854483	0.017437	0.829724	0.829867	0.017232
Sc = 3	0.944314	0.944337	0.002436	0.913169	0.913172	0.000329
$S_2 = 0.1$	0.944315	0.944337	0.002329	0.912808	0.913172	0.039861
$S_2 = 0.2$	0.875179	0.875255	0.008683	0.849065	0.849469	0.047559
$S_2 = 0.3$	0.815249	0.815292	0.005274	0.793932	0.794032	0.012594
Absolute Average error percentage			0.00939			0.016349



REFERENCES 17

Appendix A: Nomenclature

Symbol	Meaning			
ν	Kinematic viscosity			
X	Non-dimensional variable			
u_e	Velocity of free stream			
T_w, C_w	Fluid's temperature, Fluid's concentration			
G(X)	Non-dimensional temperature			
ρ	Density of the fluid			
B_0	Applied magnetic field			
K	MNF's relaxation time			
β	Deborah number/ MNF factor			
Sc, Pr	Schmidt number, Prandtl number			
τ_w, q_w, q_m	Shear stress, Heat flux, Mass flux of the surface			
T_{∞}, C_{∞}	Ambient temperature, Ambient concentration			
Nt, Nb	Thermophoresis factor, Brownian motion coefficient			
Н	Heat source factor			
S_1, S_2	Thermal slip factor, Concentration slip factor			
Nu_x, Sh_x	Nusselt number, Sherwood number			
D_T	Coefficient of thermophoresis diffusion			
ϵ	Coefficient of mass transmission			
λ	Shrinking sheet factor			
P(X)	Non-dimensional concentration			
Γ	Time constant			
Q, γ	Chemical reaction factor, Williamson fluid factor			
F'(X)	Non-dimensional velocity			
Re_x	Local Reynolds number			
M, R	Magnetic factor, Radiation factor			
C_{f_x}	Skin friction factor			
MHD	Magnetohydrodynamic			
HAM	Homotopy analysis methodology			
MHAM	Modified homotopy analysis methodology			

References

- [1] V. Ananthaswamy, R. R. Subanya, and S. Sivasankari, A mathematical study on a steady MHD flow in double stratification medium, CFD Letters, 15(10) (2023), 34-51.
- [2] N. A. Azmi, M. R. Ilias, S. S. Ishak, R. Osman, A. Rahman, Maxwell hybrid nanofluid flow towards a stagnation point on a stretching/shrinking inclined plate with radiation and nanoparticles shapes effect, J. Adv. Res. Num. Heat Trans., 1(1) (2024), 1-16.
- [3] K. Bhattacharyya, Effects of radiation and heat source/sink on unsteady MHD boundary layer flow and heat transfer over a shrinking sheet with suction/injection, Front. Chem. Sci. Eng., 5(3) (2011), 376–384.
- [4] M. Bilal, I. Siddique, A. Borawski, A. Raza, M. Nadeem, and M. Sallah, Williamson magneto nanofluid flow over partially slip and convective cylinder with thermal radiation and variable conductivity, Sci. Reports, 12(1) (2022), 12727.
- [5] N. Faraz, and Y. Khan, Thin film flow of an unsteady Maxwell fluid over a shrink-ing/stretching sheet with variable fluid properties, Int. J. Num. Meth. Heat Fluid Flow, 28(7) (2018), 1596–1612.
- [6] R. Geetha, B. Reddappa, N. Tarakaramu, B. R. Kumar, and M. I. Khan, Effect of double stratification on MHD Williamson boundary layer flow and heat transfer across shrinking/stretching sheet immersed in a porous medium,



18 REFERENCES

- Int. J. Che. Eng., 2024(1) (2024), 1-12.
- [7] A. Hafeez, M. Khan, J. Ahmed, A. Ahmed, and Z. Iqbal, Flow of Oldroyd-B fluid over a rotating disk through porous medium with Soret-Dufour effects, Arab. J. Sci. Eng., 45(7) (2020), 5949–5957.
- [8] N. A. Halim, S. Sivasankaran, and N. F. M. Noor, Active and passive controls of the Williamson stagnation nanofluid flow over a stretching/shrinking surface, Neu. Comp. App., 28(2016), 1023–1033.
- [9] T. Hayat, Y. Saeed, S. Asad, and A. Alsaedi, Soret and dufour effects in the flow of Williamson fluid over an unsteady stretching surface with thermal radiation, Zeit. für Nat. A., 70(4) (2015), 235–243.
- [10] M. A. Iqbal, M. Usman, F. M. Allehiany, M. Hussain, and K. A. Khan, Rotating MHD Williamson nanofluid flow in 3D over exponentially stretching sheet with variable thermal conductivity and diffusivity, Heliyon, 9(11) (2023), e22294.
- [11] P. K. Kameswaran, M. Narayana, P. Sibanda, and P. V. S. N. Murthy, Hydromagnetic nanofluid flow due to a stretching or shrinking sheet with viscous dissipation and chemical reaction effects, International Journal of Heat and Mass Transfer, 55(25-26) (2012), 7587-7595.
- [12] Z. Khan, H. U. Rasheed, T. A. Alkanhal, M. Ullah, I. Khan, and I. Tlili, Effect of magnetic field and heat source on Upper-convected-Maxwell fluid in a porous channel, Open Phy., 16(1) (2018), 917–928.
- [13] Y. B. Kho, A. Hussanan, M. K. A. Mohamed, N. M. Sarif, Z. Ismail, and M. Z. Salleh, Thermal radiation effect on MHD Flow and heat transfer analysis of Williamson nanofluid past over a stretching sheet with constant wall temperature, J. Phy., 890(1) (2017), 012034.
- [14] Y. X. Li, M. H. Alshbool, Y. P. Lv, I. Khan, M. Riaz Khan, and A. Issakhov, Heat and mass transfer in MHD Williamson nanofluid flow over an exponentially porous stretching surface, Case St. Ther. Eng., 26 (2021), 100975.
- [15] S. J. Liao, A Analytic solutions of the temperature distribution in blasius viscous flow problems, J. Fluid Mech., 453 (2019), 411–425.
- [16] S. J. Liao, An approximate solution technique which does not depend upon small parameters: a special example, Int. J. Non-Linear Mech., 30 (1995), 371–380.
- [17] S. J. Liao, An explicit totally analytic approximation of Blasius viscous flow problem, Int. J. Non-Linear Mech., 385 (1999), 385.
- [18] S. J. Liao, Proposed homotopy analysis techniques for the solution of non-linear Problems, Ph.D. dissertation, Shanghai Jiao Tong University, Shanghai, (1992).
- [19] S. J. Liao, A uniformly valid analytic solution of 2D viscous flow past a semi-infinite flat plate, J. Fluid Mech., 385 (1999), 101–128.
- [20] S. A. Lone, S. Anwar, Z. Raizah, P. Kumam, T. Seangwattana, and A. Saeed, Analysis of the Time-Dependent magnetohydrodynamic Newtonian fluid flow over a rotating sphere with thermal radiation and chemical reaction, Heliyon, 9(7) (2023).
- [21] J. C. Maxwell, On the dynamical theory of gases, Philo. Trans. Royal Soc. London 157 (1867), 49–88.
- [22] S. Nadeem, R. U. Haq, and Z. H. Khan, Numerical study of MHD boundary layer flow of a Maxwell fluid past a stretching sheet in the presence of nanoparticles, J. Taiwan Inst. Chem. Eng., 45(1) (2014), 121–126.
- [23] S. Nadeem, and S. T. Hussain, Heat transfer analysis of Williamson fluid over exponentially stretching surface, App. Math. and Mech., 35(4) (2014), 489–502.
- [24] A. Ramar, A. Arulmozhi, S. Balamuralitharan, I. Khan, F. Hajjej, M. Khuthaylah, and A. Singh, *Melting heat effect in MHD flow of Maxwell fluid with zero mass flux*, Case St. in Th. Eng., 53 (2024), 103910.
- [25] G. K. Ramesh, and B. J. Gireesha, Influence of heat source/sink on a Maxwell fluid over a stretching surface with convective boundary condition in the presence of nanoparticles, Ain Shams Eng. J., 5(3) (2014), 991–998.
- [26] S. K. Saini and R. Agrawal, A comparative analysis of the stagnation point flow of Williamson and Maxwell nanofluid over shrinking surface with heat source, thermal and concentration slip: Galerkin weighted residual Approach, Thermal Advances, 1 (2024).
- [27] M. Saleem, and M. Hussain, Impression of nonlinear radiation and Stefan blowing on the magneto cross nano-Williamson fluid above exponentially stretching sheet, Results Eng., 17 (2022), 100864.
- [28] S. Sivasankari, and V. Ananthaswamy, A mathematical study on non-linear ordinary differential equation for Magnetohydrodynamic flow of the Darcy-Forchheimer nanofluid, Computational Methods for Differential Equations,



REFERENCES 19

- 11(4) (2023), 696-715.
- [29] R. R. Subanya, V. Ananthaswamy, and S. Sivasundaram, Semi analytical expressions of a non-linear boundary value problem for free stream MHD flow with the effect of velocity slip condition, Mathematics in Engineering, Science & Aerospace (MESA), 13(2) (2022), 805-819.
- [30] K. Swain, S. M. Ibrahim, G. Dharmaiah, and S. Noeiaghdam, Numerical study of nanoparticles aggregation on radiative 3D flow of Maxwell fluid over a permeable stretching surface with thermal radiation and heat source/sink, Results Eng., 19 (2023), 101208.
- [31] A. B. Vishalakshi, U. S. Mahabaleshwar, and I. E. Sarris, An MHD fluid flow over a porous stretching/shrinking sheet with slips and mass transpiration, Micro., 13(1) (2022), 116 44.
- [32] R. V. Williamson, The flow of pseudo plastic materials, Ind. Eng. Chem., 21(11) (1929), 1108–1111.



